Aerospace Science and Technology ••• (••••) ••••••

Contents lists available at ScienceDirect

Aerospace Science and Technology

www.elsevier.com/locate/aescte

Effects of the foam metal casing treatment on aerodynamic stability and aerocoustic noise in an axial flow compressor

Dakun Sun [a], Jia Li [a], Ruize Xu [a], Xu Dong [b,*], Dan Zhao [c], Xiaofeng Sun [a]

[a] School of Energy and Power Engineering, Beihang University, No. 37 Xueyuan Road, Haidian District, Beijing 100191, People's Republic of China
[b] Research Institute of Aero-Engine, Beihang University, No. 37 Xueyuan Road, Haidian District, Beijing 100191, People's Republic of China
[c] Department of Mechanical Engineering, College of Engineering, University of Canterbury, Private Bag 4800, Christchurch 8140, New Zealand

ARTICLE INFO

Article history:
Received 3 December 2020
Received in revised form 15 March 2021
Accepted 30 April 2021
Available online xxxx
Communicated by Yongle Du

ABSTRACT

A kind of foam metal casing treatment (FMCT) is proposed and experimentally tested on a low-speed axial flow compressor in this work. Foam metal is a foam-like substance with a lightweight structure but a certain strength. Both time-mean and high-response instrumentation are applied to capture the steady and unsteady performances of the compressor. Initially, parametric experimental measurements on axial location of foam metal over rotors are performed with respect to stability enhancement and noise reduction. It is found that the stall margin improvement (SMI) and the aerodynamic efficiency loss are functions of the axial location of the foam metal. Particularly, the SMI maxima appears at CT7 with a certain amount of aerodynamic efficiency loss. In analyzing the results measured over and downstream of the rotor, it is suggested that the release of rotor tip loading may be a stability improvement mechanism of FMCTs. Furthermore, comparison in the stall inception process of the axial flow between the compressor with the solid-wall and the implementation configuration shows that, in solid-wall casing condition, the compressor experiences a spike-type stall inception, however in CT7, the compressor goes through a modal-type process. Finally, conclusions and suggestions are given based on the findings.

1. Introduction

Recent development trends in aero-engine include increasing thrust-weight ratio and decreasing noise emission. As a result, there are at least two problems should be considered: First, demand on higher thrust-weight ratio leads to a significant increase of stage aerodynamic loading for reduced numbers of compressor stage, which will result in a higher tendency of rotating stall, i.e. the stall margin is reduced. Second, aero-engine nacelles are expected to be shortened to reduce weight and drag. However the shortened nacelles will supply less treatment area for acoustic liners. So the noise attenuation from inlet liners is correspondingly decreased.

Historically, the two problems mentioned were solved separately. In terms of stall margin improvement, many attempts including active control [1] tip air injection [2] and casing treatment [3,4] have been made to address this issue. In particular, continuing researches on active control technology have been performed for many years since it was reported by Epstein et al. [1]. A useful increase in stall margin was achieved by controlling variable vanes or fast-acting air jets [5–7]. However, due to the elusory stall inception patterns and sophisticated control system, active control technology is far from ready for practical applications [8,9]. On the other hand, casing treatments, originally proposed by NASA, have received steady interest for more than 50 years [10]. Initially attention was focused on finding perfect casing treatment configurations which were beneficial to stall margin improvement. A quantity of configurations involving slots, grooves, straight holes and honeycombs were experimentally tested in both low-speed and high-speed compressors [3,11]. It was found that different casing treatment configurations imposed various effects on compressor performance. Generally, slot-type casing treatment configurations are highly regarded for generating significant stall margin improvement. At the same time, a common conclusion drawn from numerous investigations was that those casing treatments which successfully improved stall margin were always associated with some penalty in efficiency [12,13]. The working mechanism of casing treatments has therefore received lots of attention around the world. Takata and Tsukuda [14] experimentally measured the flow through the blade passage as well as in the slots of the casing treatments. They found that in general the static pressure at the

* Corresponding author.
E-mail address: buaadongxu@buaa.edu.cn (X. Dong).

https://doi.org/10.1016/j.ast.2021.106793
1270-9638/

Nomenclature

C_{ax}	Axial chord of rotor tip
C_p	Casing pressure coefficient
C_{pt}	Total pressure coefficient
C_{vx}	Axial velocity coefficient
CT^*	FMCT with foam metal at location * in the casing
FM	Foam metal
FMCT	Foam metal casing treatment
IL	Insertion loss
PPI	Pores per inch
PSD	Power spectrum density
p_r	Reference pressure
P_{shaft}	Shaft power
P_{sw}	Casing static pressure
ΔP_{ts}	Total-to-static pressure rise
ΔP_t	Total-to-total pressure rise
Q_v	Volume flow rate
RMS	Root-mean-square
SC	Solid-wall casing condition
SPL	Sound power level
SMI	Stall margin improvement
TLV	Tip leakage vortex
U_m	Mid-span blade tangential speed
V_x	Axial velocity at inlet
X	Axial distance between foam metal rear surface and leading edge of rotor
X/C_{ax}	Normalized location of foam metal
η	Efficiency
φ	Flow coefficient, $\varphi = V_x/U_m$
ρ	Air density
ψ	Pressure rise coefficient
$\Delta\eta$	Efficiency loss

Subscript

d	At the design point
s	At the stall point
CT	FMCT condition
SC	Solid-wall casing condition

rear of the blade was higher than that in front part. When casing treatment was installed, the flow near the rear part of the slot was pushed into chamber and in turn penetrated main flow as a high speed jet at the front end, which resulted in the transfer of the momentum between the moving wall and the low momentum flow near the casing (in relative coordinate system). They further concluded that the momentum interchange plays an essential role in delay of rotating stall. Detailed measurements of flow phenomena were also performed between the blade passage, behind the rotor and inside the slots by Smith and Cumpsty [15]. They noted that the rapid growth of the blockage appeared near the pressure surface accounts for the initiate instability. The stabilizing effect of casing treatment they observed is the extraction of the blockage. Another encouraging work was concentrated on a vaned recessed casing treatment applied in a low-speed fan with aerospace type loading [16–18]. Results from parametric study presented that in some configurations significant improvements in stall margin were obtained without any loss in efficiency [16]. Further research carried out by Ziabasharhagh et al. [17] demonstrated that these casing treatment configurations were capable of strengthening the inlet distortion tolerance. Kang et al. [18] made a more detailed measurements of flow behavior near the casing wall as well as in the casing treatment. Based on measured results, they hypothesized that casing treatment modifies the leakage flow by eliminating the tip vortex, which is the main stall delay mechanism. More emphasis has recently been put on the blade tip flow which is believed to be closely related to the stall inception process in turbomachinery [19,20]. Vo et al. [21] proposed two necessary criteria for the spike-type inception, one is spillage of tip leakage flow at the leading edge and the other is backflow at the trailing edge. Stall delay mechanism of circumferential grooves is mostly thought to be associated with modifying behavior of the tip clearance flow [22–25]. A basic conclusion made from numerical and experimental studies is that groove delays the upward movement of the tip leakage flow. This is consisted with the analysis made by Shabbir et al. [26] that groove augments the wall shear stress to tolerate the higher blade loading. However Houghton and Day [27] argued that mechanism goes different in locations near the leading edge and mid-chord over the blade. Especially at mid-chord the stall margin improvement is resulted from the fact that the tangential velocity of near-casing flow is increased. More recently, another casing treatment mechanism based on suppression of stall precursor was proposed and validated by Sun et al. [28–30] and Dong et al. [31]. In general, flow disturbances appear in pre-stall process are believed to play an important role in stall onset. And these disturbances which actually trigger the final rotating stall are called stall precursors [32–34]. They designed a casing treatment consists of a backchamber and a perforated plate (the open area ratio is usually less than 12%). The casing treatment is thought to create an unsteady boundary to influence the generation and development of stall precursors.

On the other hand, in solving the problem of decreased noise reduction caused by shortened nacelles, plenty of projects including lip liner, active noise control and over-the-rotor (OTR) liner have been explored over the recent decades [35–39]. The lip liner technology is an attractive option to improve noise attenuation efficiency [35]. It is reasonable to expect this technology to be applied in industries after overcoming the challenges from icing protection and aerodynamic consideration. The OTR liner is an acoustic treatment integrated into the fan casing near the rub strip area. Sutliff et al. [36,37] first proposed and evaluated foam metal OTR liners in both low-speed and high-speed fan rigs, respectively. Research results suggested a 4 dB broadband noise reduction in low-speed machine. Based on the measurements they concluded that the noise reduction mechanism of OTR was a combination of acoustic attenuation and source modification. In subsequent investigations the OTR liner was designed employing perforated groove for aerodynamic purposes [40]. More recently, experiments were also conducted in a grazing flow impedance tube to determine the acoustic characteristic of the grooved OTR liner [41] and an analytical model [42] was also deduced to predict the sound attenuation with OTR liner. We believe that more encouraging works will be further reported with more understanding of OTR acoustic liners.

Although considerable studies of the stall margin-improving technology as well as the fan/compressor noise-reducing technology have been performed for decades, there has been little experimental evidence of an alternative treatment method which works in these two aspects. The dual-effect technology mentioned may be of great concern due to the increasing desire for higher thrust-weight ratio. This motivated the present work. In this work, we propose a kind of foam metal casing treatment (FMCT) and experimentally evaluate its effects in stability enhancement and aeroacoustic noise reduction in a low-speed compressor. This paper is organized as follows: Firstly, the experimental apparatus and

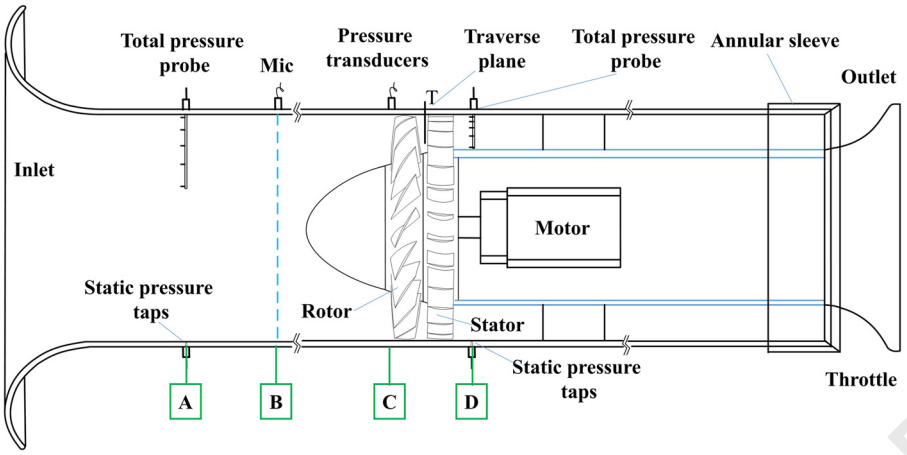

Fig. 1. Test compressor TA36 and measurement setup.

Table 1
Design specifications of TA36.

	Rotor	Stator
No. of blades	20	27
Stagger angle at tip (°)	60	7
Aspect ratio	1.18	1.40
Hub-to-tip ratio	0.577	0.669
Casing diameter (mm)	600	
Design flow coefficient	0.24	
Design pressure rise coefficient	0.48	
Design operation speed (rpm)	2930	
Rotor tip axial chord (mm) C_{ax}	50	

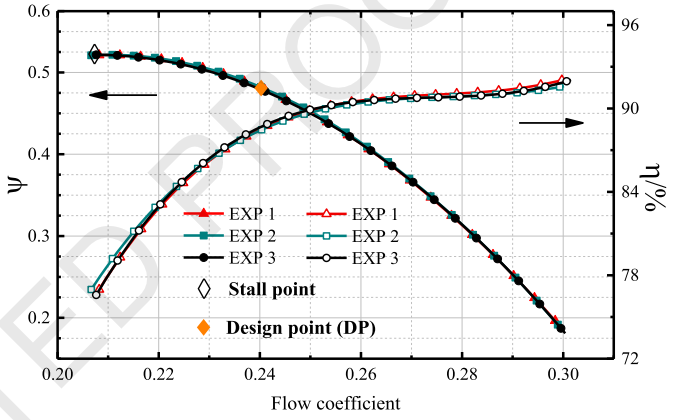

Fig. 2. Repeated characteristics of TA36 in solid-wall casing. (For interpretation of the colors in the figure(s), the reader is referred to the web version of this article.)

measurement device are introduced. Secondly, a parametric study is carried out to find the optimum location of the foam metal in casing in terms of SMI, efficiency loss and noise attention. A mechanism is also proposed and discussed. Thirdly, conclusions are drawn based on experimental measurements.

2. Test rig and measurement setup

2.1. The test compressor

The experimental investigation was performed on a single-stage axial-flow compressor, the TA36. A schematic view of the TA36 is shown in Fig. 1. It was driven by a servo motor embedded in the hub and the rotor speed can be continuously varied up to the value required. The air was drawn into the compressor from a large room at a steady atmosphere conditions. The mass flow through the whole compressor was controlled by an annular sleeve which was powered using a stepping motor. The rotor tip tangential speed in the present experiment was 90.8 m/s indicating that the flow can be considered as incompressible. The design characteristics of the compressor are summarized in the Table 1.

2.2. Experimental equipment and definition of key parameters

Both time-averaged and fast-response transducers were adopted to evaluate the steady characteristics as well as unsteady features of the TA36 compressor. Specifically, the atmospheric temperature was measured using a mercury thermometer and the atmospheric pressure was given by a standard mercury barometer. Steady pressures were measured by Honeywell pressure transducers and unsteady pressures were obtained by Kulite 190 high-frequency pressure transducers.

To measure steady characteristics, two radial rakes of five total pressure probes were used, one was mounted in the compressor's inlet duct (Plane A) to provide the averaged total pressure of the upstream air and the other one was placed at 50 mm downstream of the stator (Plane D) to measure the total pressure of the outflow. Additionally at both locations, there were four casing tappings equally spaced around the circumference to obtain the static pressure. In particular, static pressure measured in the inlet bellmouth provided the input for calculating the flow coefficient and the downstream measurements were used to determine the pressure rise characteristics ψ which is defined as

$$\psi = \frac{\Delta P_{ts}}{1/2\rho U_m^2} \tag{1}$$

where the ΔP_{ts} is the total-to-static pressure rise over whole stage, ρ is the density of the air and U_m is the tangential speed at the blade midspan. In the present experiment, the efficiency η was calculated from the total pressure rise over the stage and the shaft torque power, which is expressed as

$$\eta = \frac{Q_v \Delta P_t}{P_{shaft}} \tag{2}$$

Repeated total-to-static pressure rise and efficiency characteristics of TA36 compressor are plotted in Fig. 2. The solid orange diamond refers to the design point (DP) and the hollow diamond represents the stall point. Note that the stall point here refers to the last stable operation point of the compressor along the characteristic curves. The measurements present a good repeatability.

The compressor stability was evaluated using the comprehensive stall margin (SM) in terms of pressure rise and flow coefficient at design point and stall point, respectively. The SM is defined as

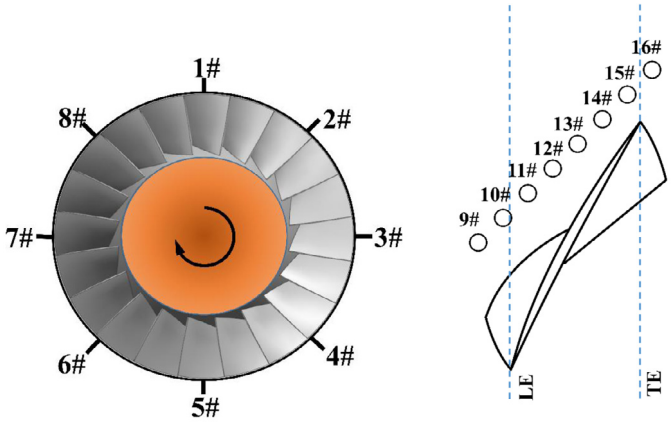

(1) circumferential array (2) chord-wise array

Fig. 3. Schematic layout of high-frequency transducers.

$$SM = \left(\psi_s/\varphi_s \Big/ \psi_d/\varphi_d - 1\right) \times 100\% \quad (3)$$

where the subscript d and s indicates the design point and the stall point, respectively.

A total of 16 high-frequency flush-mounted transducers were employed to measure unsteady static pressures near the casing wall. In particular, the first set of eight transducers were positioned $0.4C_{ax}$ (Fig. 1, Plane C) ahead of rotor leading edge and spread equally along the circumference of the annulus to detect the pre-stall process. Additionally, for measuring the casing wall pressure distribution over the rotor tip, the other eight transducers were mounted on the casing covering the measure points from 9 mm ($0.18C_{ax}$) upstream of the rotor leading edge to 7 mm ($0.14C_{ax}$) downstream of the trailing edge axially (shown in Fig. 3). The Photoelectric Switch Sensor was used for phase locking when acquiring the dynamic data and the ensemble averaged measurements at the same spatial position during every rotor revolution can be taken. The sampling frequency was 50K Hz resulting 51 sample points per blade passage.

Flow conditions behind the rotor were measured by a five-hole pressure probe. The probe was 2 mm in diameter and fixed on a traverse gear. Radial traverse contains 30 points with 3 mm intervals. Generally, circumferential-averaged flow angle, three dimensional velocity, static pressure and total pressure can be obtained at the $0.33C_{ax}$ downstream of the rotor trailing edge (Fig. 1, Position T). The probe was calibrated with a wide range angles of Mach numbers, which is enough to cover the operating conditions considered in the present experiments.

In order to evaluate the acoustic benefits of the FMCT, a circumferential array of twenty equally spaced 1/4 inch microphones (G.R.A.S type 40BH) was flush placed 605 mm upstream of the rotor face (Fig. 1, Plane B). And sound energy obtained from these microphones were averaged to reduce the random signal. The acoustic signals were measured at the design point of the compressor in solid-wall casing condition (SC). In particular, the insertion loss (IL) was used to evaluate the noise reduction quantitatively. The IL is calculated from

$$IL = SPL_{SC} - SPL_{CT} \quad (4)$$

the subscript SC and CT refers to conditions in solid-wall casing and FMCT, respectively. The SPL in the formula is the sound pressure level and defined as

$$SPL = 20\log\left(p/p_r\right) \quad (5)$$

in which the reference pressure p_r is 2×10^{-5} Pa.

Table 2
Foam metal location for eight FMCTs.

FMCT	CT1	CT2	CT3	CT4	CT5	CT6	CT7	CT8
X/C_{ax}	0	0.1	0.2	0.3	0.4	0.5	0.6	0.7

2.3. The foam metal casing treatment (FMCT)

Foam metal is a foam-like substance which is widely applied in flow control, vibration damping and acoustic absorption mainly based on their physical properties [43]. Figuratively, the foam metal resembles a sponge material with a plenty of small interlinked cavities. It is characterized by PPI (Pores Per Inch). The advantage of using foam metal as a casing treatment is obvious: low density with good shear and fracture strength, good fire resistance, self-supporting due to its rigidness and strength, low moisture absorption, and so on. These advantages allow foam metal to survive near or over the rotor, which is a very harsh pressure and temperature environment. In the present experiment, the foam metal used is made using ferronickel and its PPI is 35.

The FMCT consists of a foam metal ring and a casing configuration. Specifically, the foam metal ring was manufactured in three identical segments, each of which was a one-third arc of the whole circumference. The axial length and the radial thickness of the foam metal ring are 25 mm ($0.5C_{ax}$) and 20 mm ($0.4C_{ax}$), respectively, resulting an aspect ratio of 0.8. The location of the foam metal in casing is defined as the axial distance from the foam metal rear face to the rotor tip leading edge. As depicted in Fig. 4, the farthest location numbered as 8 was at $0.7C_{ax}$ (35 mm) downstream of the rotor leading edge. The FMCTs tested in the present experiment are summarized in Table 2. Axial location change of the foam metal ring at the interval of $0.1C_{ax}$ was achieved by employing a set of resin shims, which allows to investigate the impact of single foam metal ring at different locations on compressor stability and noise.

3. Parametric study of the FMCT

3.1. Stability enhancement

This section investigates the impact of the foam metal's axial location on FMCT's performance. For brevity, each configuration is distinguished by the combination of CT and location number. For example, CT1 refers to a FMCT configuration with foam metal placed in location 1 defined.

The compressor characteristics were measured by throttling the operating point slowly from choke point up to the stability limit and setting back quickly from the rotating stall. Every step can be considered as the quasi-steady behavior during the entire period. Back-to-back tests were also performed to ensure the reliable data. Basically, two characteristic parameters are of great concern: one is the stall margin improvement (SMI) and another is the efficiency loss ($\Delta\eta$). To note that the efficiency loss is the percentage reduction caused by the FMCT at the design point of the compressor.

The pressure rise and efficiency characteristics measured with and without FMCTs are presented in Fig. 5. For clarity, only two typical characteristics obtained with SC and CT7 are given, respectively. The design point and stall points in two cases are also marked. No distinctive change can be seen until to reaching the stall point in SC. As shown in pressure rise characteristics, with CT7 the compressor is capable of operating at a lower flow rate but higher pressure point and the calculated SMI is 36.1%. In efficiency characteristics, two features should be noted. First, at some larger flow rates, efficiency loss caused by FMCTs are negligible. Second, at the design point, efficiency is reduced by 1.5% with CT7.

The SMI as well as the efficiency loss as functions of foam metal locations are summarized in Fig. 6. The upper graph is the SMI

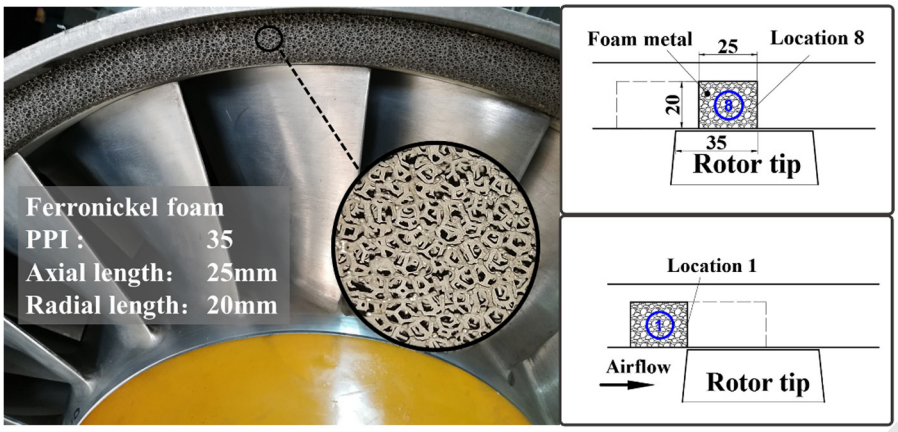

Fig. 4. Configuration of FMCT with foam at different locations.

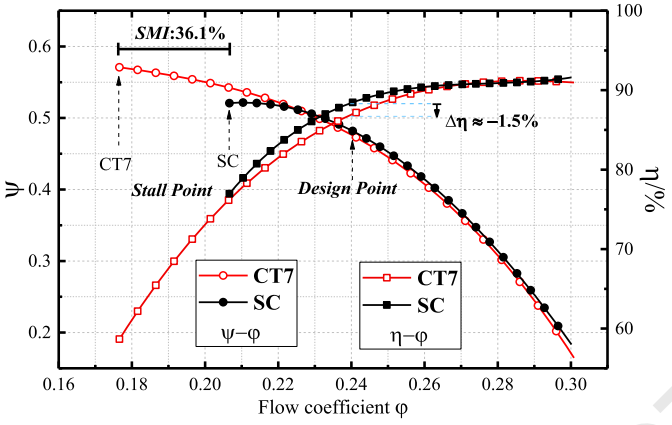

Fig. 5. Comparison in characteristics of compressor in SC and CT7.

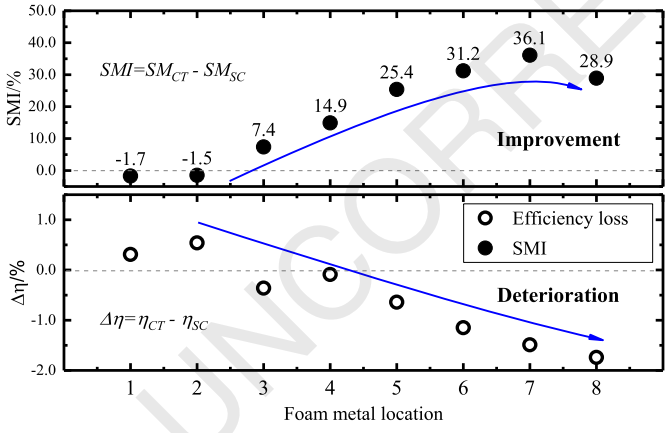

Fig. 6. SMI and efficiency loss at each foam metal location.

versus locations and the lower one is related to the efficiency loss. Generally, the SMI tends to increase when the foam metal is installed at a place more downstream of the leading edge and the efficiency loss shares the same rule. There seems to be an optimum foam metal location at CT7 that $0.6C_{ax}$ downstream from the rotor leading edge, but a little more efficiency loss is also found at this location.

In the following sections, attention will be focused on CT7 to find the mechanism accounting for the SMI and efficiency loss caused by FMCTs.

3.2. Comparison in casing static pressure distribution

The first concern is put on the tip clearance flow due to the fact that the flow behavior near endwall is believed to be greatly related to compressor stability [32,33]. On the other hand, the foam metal interacts directly with the flow field in this region. The casing static pressure P_{sw} is nondimensionalized by the dynamic pressure and presented as the casing pressure coefficient C_p:

$$C_p = \frac{P_{sw} - P_{t1}}{1/2\rho U_m^2} \tag{6}$$

Comparison of static pressure contours was made between conditions with SC and CT7 at two operation points, one flow coefficient is 0.24 (the design condition, labeled by DP) and another is 0.21 (the near stall condition in SC, labeled by NP), respectively. In the Figs. 7, 8 and 9, for clarity, the leading edge and the trailing edge of rotor tip are labeled with LE and TE, respectively. Additionally, the axial location of the foam metal was also marked using a dashed box.

In Fig. 7, generally speaking, two types of flow are of interest. One is the incoming flow inpouring the blade passage. Another concern is the tip leakage flow, driven by the pressure difference between the pressure and the suction sides of the blade, leaks over the tip gap and induces some reversed flow against the incoming flow. The strongest tip leakage flow is thought to be formed at the position of the maximum pressure difference between the two sides of the blade. Mostly, the leakage flow, bounded by the casing, will interacts with the incoming flow and some other secondary flows, hence to roll up into a vortex [44]. The trajectory of the vortex can be recognized by the pressure trough originating from the core of the lowest pressure region near the peak suction side [45] and is indicated by a red arrow in each graph. At DP, in SC, the tip leakage vortex trajectory (TLV) originates at about 8% axial chord of rotor suction side and extends towards the center of blade passage subsequently. However in CT7, the TLV is seen stay closer to the blade surface than that in SC and turns to passage center at a further backward position. It is known that the behavior of the TLV is mainly resulted from the momentum balance between the incoming flow and the leakage flow. Normally, as the flow coefficient is reduced, the blade loading (pressure difference between the two sides of the blade) increases and the momentum of the incoming flow decreases, resulting a forward movement of the TLV. In the present case, data were measured at the same flow coefficient. The different behaviors of TLV shown in SC and CT7 are related to the different loading conditions near the rotor tip. The reason could be found in regions circled by the blue oval, especially the area covered by the foam metal, the static pressure in

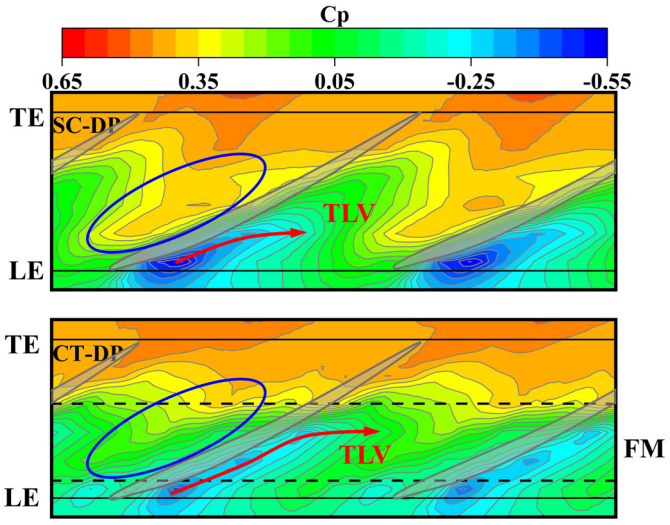

Fig. 7. Static pressure over rotor at DP for SC (up) and CT7 (down).

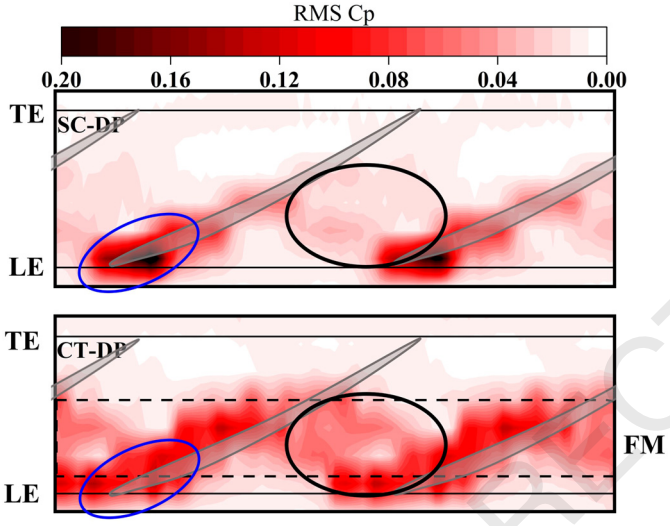

Fig. 8. RMS of static pressure at DP for SC (up) and CT7 (down).

CT7 is lower than that in SC. It is the reduced loading that is responsible for the weakened leakage flow.

The distribution of the calculated RMS C_p is given in Fig. 8. Generally, the RMS refers to the flow fluctuation and the highest RMS is thought to be corresponding to the interface between the incoming and the tip leakage flows [44]. In SC, the highest RMS is concentrated near the blade leading edge as circled by the blue oval, which indicates there exists a strong interaction between incoming and leakage flows. However in the same region of blade in CT7, the RMS value is reduced. This is because the leakage flow is reduced. Furthermore, in regions covered by foam metal, in both blade tip and passage, the RMS value is higher than that in SC. It is suspected that there may be a radial in and out movement of flow and a cross movement of TLV near the foam metal surface.

At NP, the comparison in near casing pressure distribution between cases with SC and CT7 are given in Fig. 9. As the flow coefficient decreases, the blade loading rises as shown in the figure. However, in comparison between the regions marked by the blue ovals in two cases, one can draw the same conclusion as that in DP, that the tip blade loading is reduced in CT7 situation.

This section confirms that the behavior of tip leakage flow is influenced by the FMCT. Based on the results, a basic hypothesis is that the foam metal may release the tip blade loading by allowing more flow immigrates towards the suction side or the adjacent passage. To be specific, the flow entering the foam metal reduces the pressure near the pressure surface, while the flow moving out of the foam metal increases the pressure on suction surface. Comparing the pressure difference with that in solid wall condition, the foam metal casing treatment reduces the loading of the blade. Further more, this cross movement is naturally not in line with the mainflow, which probably causes a certain amount of efficiency loss.

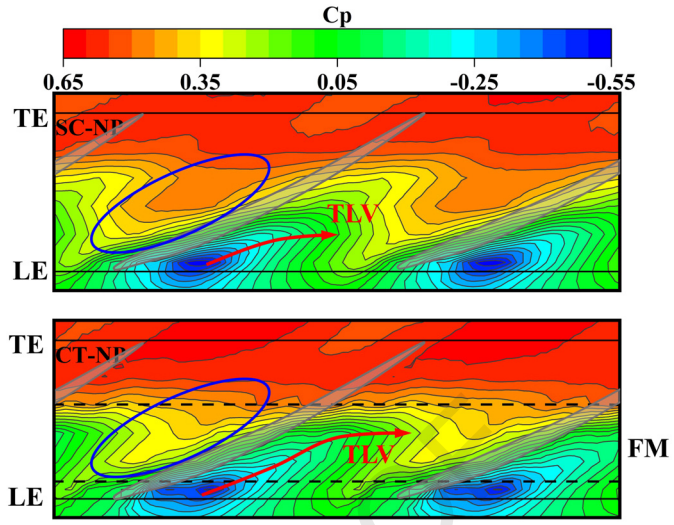

Fig. 9. Static pressure over rotor at NP for SC (up) and CT7 (down).

3.3. Comparison in radial distribution

Radial distribution of outflow from rotor was measured by a five-hole probe. This probe was traversed every 3 mm to record the local flow information. In the present experiment, distributions of total pressure and axial flow obtained at NP are presented and analyzed to further explore the working mechanism of FMCTs. In general, the total pressure represents the energy of the airflow and the axial velocity is related to the incidence angle, further refers to the blade loading. The total pressure coefficient was the nondimensionalized total pressure using the dynamic pressure. The axial velocity coefficient is defined as the ratio of the axial component of the airflow velocity to the mid-span blade tangential speed.

The left part of the Fig. 10 shows the radial distribution of the total pressure coefficient under two casing conditions. In comparing the results with SC and CT7, what can be seen is that there are some total pressure losses near the casing (about the regions above 90% span of blade) and gain in the other span when the CT7 is applied. The decreased total pressure at tip region may be corresponding to the circulated flow in and out of the foam metal surface as indicated in Fig. 7.

In the right part of the Fig. 10, differences are noticed near the 68% span of the blade, above which the axial velocity is larger than that in SC and below which the axial velocity is smaller than that in SC.

Taking these two indexes into consideration, one can conclude that, in treated condition, first, blade loading is decreased in regions upper than 68% of span and increased in the other regions. Second, the loss is increased in regions upper than 90% of span and decreased in regions from 68% to 90% spans of blade. Based on the analysis above, it is suspected that the increased loss is caused by the radial movement of flow and the decreased loss is corresponding to that the blockage in this region is suppressed.

In addition, one can find that in treated cases, the radial distribution of blade loading is shifted. Specifically, the loading in upper

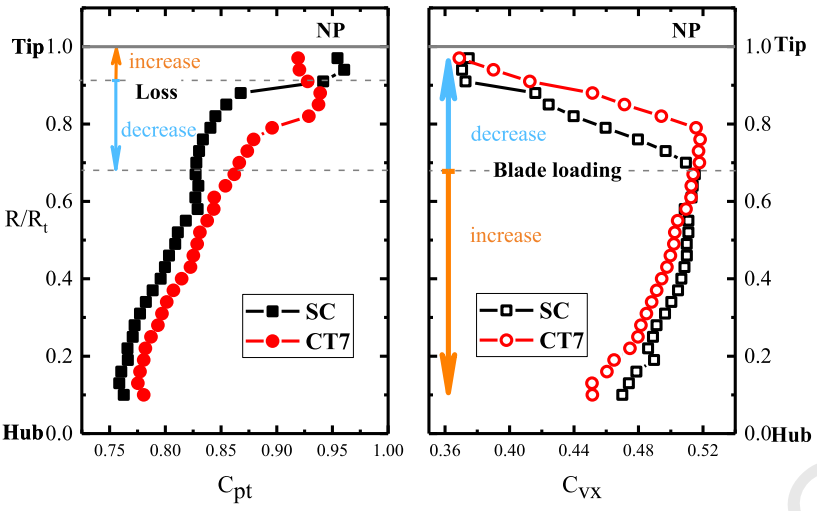

Fig. 10. Radial measurements downstream rotor at NP for SC and CT7.

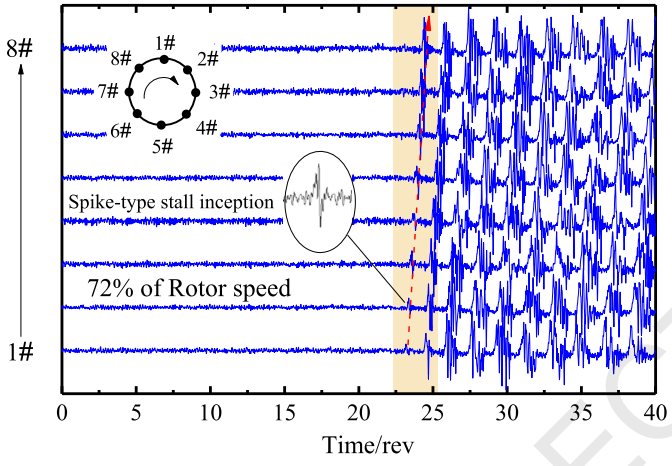

Fig. 11. Static pressures obtained from the circumferential transducers in SC to show a spike-type stall inception process.

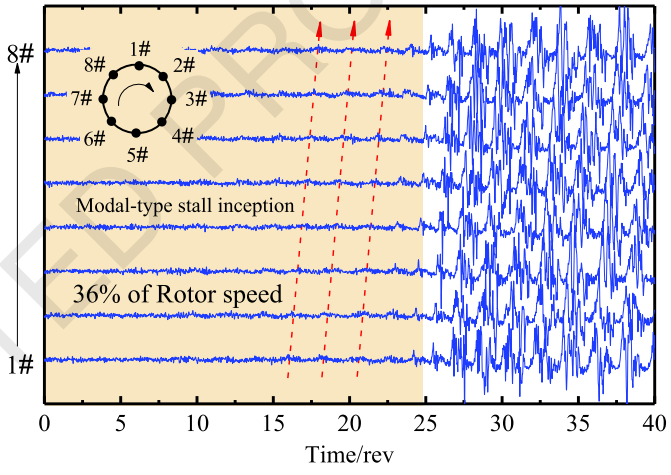

Fig. 12. Static pressures obtained from the circumferential transducers in CT7 to show a modal-type stall inception process.

span is reduced however that in lower span is increased. It is thus implied that the stall inception may be influenced by FMCTs. This concern will be verified in the next section.

4. Stall inception analysis

Previous tests showed that the TA 36 compressor is a spike-type stall inception machine (Fig. 11). When compressor was throttled very close to the stall point, a spike emerged and rapidly developed into a rotating stall cell. As shown in Fig. 11, a spike grows into stall cell in a few revolutions.

As the same method used in SC, stall inception process of compressor with CT7 was measured by eight high-frequency transducers equally mounted along the circumferential direction at the upstream of the leading edge. As shown in Fig. 12, a weak long-scale precursor wave is observed before stall. To give a further evidence, the power spectrum analysis for the first spatial harmonic of the measured data during the period before 20 revolutions prior to stall was performed and shown in Fig. 13. Clearly, a dominant wave traveling at about 36% of the rotor speed is presented.

A clear stall inception comparison is given in Fig. 14. The gray and blue curves represent the original and filtered data, respectively. Note that the filtered data is obtained using Fourier 5-800 Hz band-passing filtering method. The modal wave is seen several rotor revolutions before stall as indicated by a dash box in

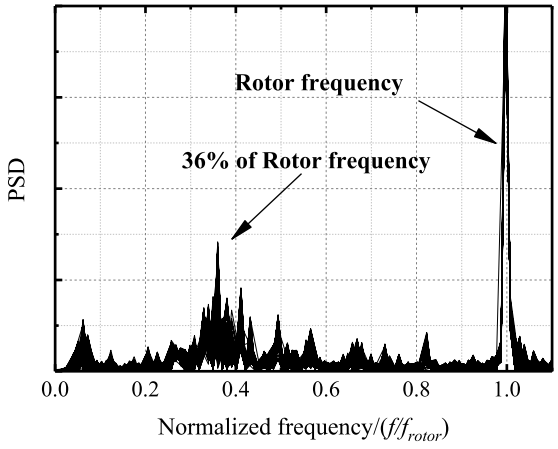

Fig. 13. PSD results of the first spatial harmonic of the measured data during the period before 20 revolutions prior to stall.

CT7 condition. As stated by Camp and Day [20] spike is a localized flow separation at the rotor tip region while the modal wave is an oscillation of the flow field. In treated case, the axial velocity near the rotor tip is increased resulting in a reduced loading or incidence. In consequence the critical incidence for the spike is loosed

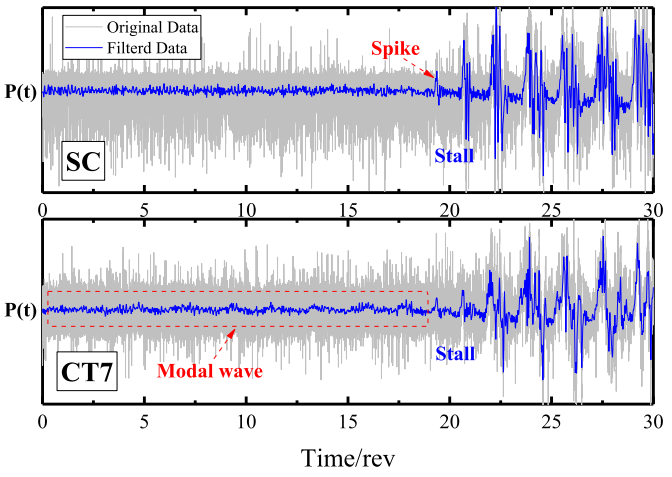

Fig. 14. Comparison in stall inception process for SC and CT7.

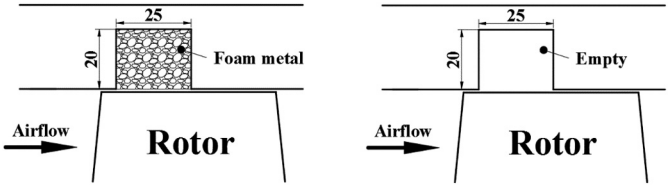

Fig. 15. A schematic view of CT7 (left) and G7 (right).

to a larger scale. Or from a system point of view, the spike-type precursor is suppressed at these flow coefficients. In consequence, at NP, the compressor with CT7 is operating stably.

Based on the results above, a stall scenario in CT7 can be proposed. Started from NP, with further throttling, the loading of the rotor blade (especially in the lower span) is increasing. Once the new stability limit of the compressor system is achieved, modal wave stall inception occurs.

5. Effect of the "left" groove on compressor stability

To go one step further, one may interest in such a situation where the CT7 is replaced by a single groove, i.e., only a 20*25 empty groove is assigned at the location 7 as shown in Fig. 15. If the effect of FMCTs on compressor stability is only to release the rotor tip loading, the left circumferential groove is supposed to generate some SMI. The characteristic results obtained in "grooved" casing treatment is illustrated in Fig. 16. For clarity, the treated case that groove in location 7 is represented by G7. The left ordinate is the pressure rise coefficient and the right ordinate is the efficiency. The solid symbol refers to conditions in SC while the open symbol corresponds to that in G7. It is found that the compressor will stall earlier in G7 than that in SC, which indicates that the groove itself (in the present length-width scale) is failed to improve the compressor performance. In addition, the efficiency at the design point is reduced by 2.7% in G7. It is implied that the groove may be too large that the flow in it is disorderly.

The view presented here of the results with and without foam metal in groove indicates that the physical property like flow resistance is also important. The airflow is restricted in foam metal rather than the open space in which the flow moves more freely. Hypothetically, in grooved case, the flow structure near the casing is that part of the leakage flow penetrates into groove at rear part of groove, and the flow inside the groove will be pushed out of groove at the front part [23]. At the same time, the other leakage flow moves across over the tip clearance as it does in the SC condition. The thing different in grooved case is that the shear force

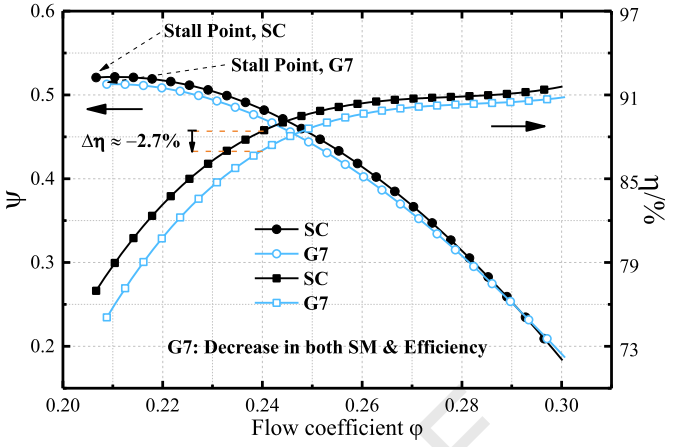

Fig. 16. Comparison in characteristics of compressor in SC and G7.

generally caused by solid-wall casing is absent. Consequently, the tip leakage flow accelerates though the tip clearance almost in the tangential direction. Further, to fill the groove with foam metal, the foam metal acts as a soft boundary. The leakage flow is thought to share the same features as it has in groove, i.e. the upper part enters into the foam metal and the lower part flows over the tip clearance. For one thing, cross movement of the leakage flow reduces the blade loading near the tip. For another, the decreased shear force from the foamed surface results in a tangential movement tendency of leakage flow as illustrated in Fig. 7 and Fig. 9.

6. Aeroacoustic noise reduction

Foam metals used to reduce the compressor noise has been investigated for decades. This section will briefly report the noise reduction caused by FMCTs rather to discuss the noise attenuation mechanism. Previous tests showed that the emitted noise of TA36 is dominated by the rotor-stator interaction noise at the third order blade passing frequency (BPF). The typical frequency spectrum is shown in Fig. 17. The chart plotted by black line is the frequency spectrum under the SC while the red one is drawn using measurements taken under FMCTs. The ordinate is sound pressure level (SPL) and the abscissa is the frequency. It appears that the tone noise at third order BPF is attenuated by 3.2 dB in treated case. Besides, the broadband noise is suppressed in a large frequency band as circled by a dotted box.

To show a more quantitative comparison, the insertion loss (IL) is calculated based on the integrated SPL up to 8000 Hz in which band occupying the major energy of the sound. An interesting relation between the location of the foam metal and the IL is seen in Fig. 18. The IL varies in 0.18∼1.6 dB and the maxima occurs at location 4 (CT4). It is noted that, the foam metal is totally interacting with the flow field over the rotor when the foam metal is placed at location 6, 7 or 8. However, when it is placed at the other front 5 locations, in which the foam metal can only cover the rotor with its part span as shown in Fig. 4. Particularly, at location 1, the foam metal is installed exactly ahead of the rotor leading edge, resulting an IL of 1.23 dB. At locations 6, 7 and 8, the foam metal is totally exposed to the rotor, some ILs are still obtained.

7. Conclusions

A proposed foam metal casing treatment (FMCT) is experimentally evaluated on a low-speed axial flow compressor in this work. Based on the current experiments and measurements, the following findings are obtained:

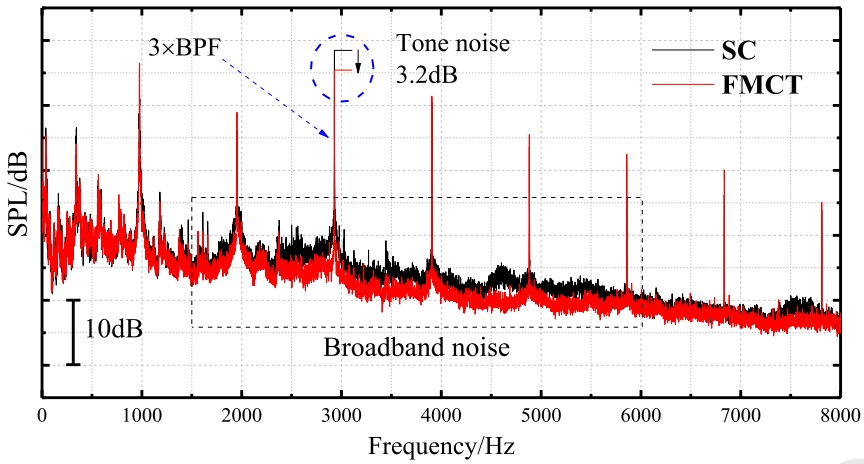

Fig. 17. Noise spectrum of compressor at DP in SC (black) and FMCT (red).

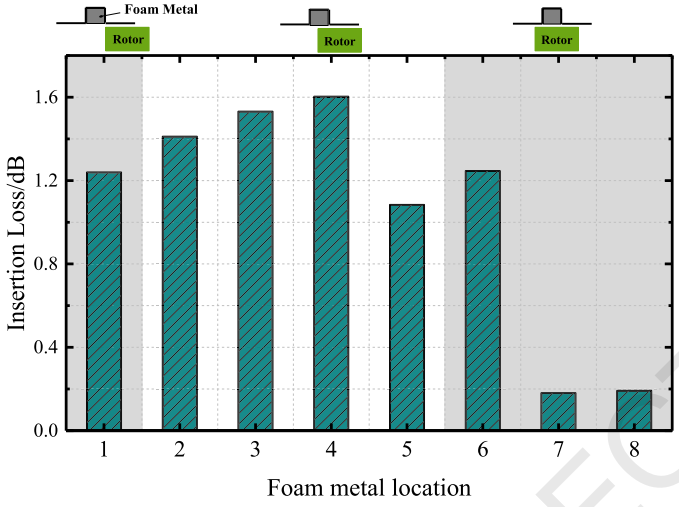

Fig. 18. Insertion loss at each foam metal location.

1 Parametric studies on the axial location of the foam metal showed that the stall margin improvement (SMI) varies in -1.5%∼36.1% and insertion loss (IL) varies in 0.18 dB∼1.6 dB.

2 Maximum improvement in stall margin is achieved in CT7 that the foam metal is located at $0.6C_{ax}$ downstream of rotor leading edge. The stall delay mechanism is thought to be the release of the blade loading near the rotor tip. The reduced tip blade loading cause an attenuated leakage flow, which influence the tip leakage vortex behavior.

3 The Foam metal casing treatment, especially CT7, changed the radial distribution of the rotor blade loading. The blade loading at the upper span is reduced and at the lower span is increased compared with that in solid-wall casing condition. It is also thought to be responsible for the conversion in stall inception.

4 The compressor is a spike-type machine in solid-wall condition, however the compressor with CT7 stalls via modal-type stall inception. It is suspected that the blade loading near rotor is reduced resulting suppression in origination of spike-type precursor. With further throttling, a new stability limits of compressor system reached and modal-type stall inception occurs.

The above findings can be of interests to designers as the foam metal casing treatment shows the potential to be applied in real aeroengines. The proposed casing treatment should be further tested in high speed or centrifugal compressors and with various inlet distortion conditions. Furthermore, rain ingestion test and icing test should be considered due to that the performance of FMCT may be influenced when water is inside or freezes on the surface of foam metal. It is also suggested that both aerodynamic and aeroacoustic effects need to be considered comprehensively in future applications.

Declaration of competing interest

The authors declare that they have no known competing financial interests or personal relationships that could have appeared to influence the work reported in this paper.

Acknowledgements

Part of this work is financially supported by the National Natural Science Foundation of China (Nos. 51822601, 51906004 and 51790514). Further thanks also go to Dr. Ming Zhang and Dr. Lin Du for insightful discussions.

References

[1] A. Eptein, J. Ffowcs Williams, E. Greitzer, Active suppression of aerodynamic instabilities in turbomachines, J. Propuls. Power 5 (2) (1989) 204–211, https://doi.org/10.2514/3.23137.
[2] J. Li, J. Du, S. Geng, F. Li, H. Zhang, Tip air injection to extend stall margin of multi-stage axial flow compressor with inlet radial distortion, Aerosp. Sci. Technol. 96 (2020) 105554, https://doi.org/10.1016/j.ast.2019.105554.
[3] M. Hathaway, Passive Endwall Treatments for Enhancing Stability, NASA Report No. TM-2007-214409, 2007.
[4] X. He, X. Zheng, Roles and mechanisms of casing treatment on different scales of flow instability in high pressure ratio centrifugal compressors, Aerosp. Sci. Technol. 84 (2019) 734–746, https://doi.org/10.1016/j.ast.2018.10.015.
[5] J. Paduano, A. Epstein, A. Valavani, J. Longley, E. Greitzer, G. Guennete, Active control of rotating stall in low speed axial compressor, J. Turbomach. 113 (4) (1993) 48–56, https://doi.org/10.1115/1.2929217.
[6] J. Day, Active suppression of rotating stall and surge in axial flow compressors, J. Turbomach. 115 (1) (1993) 40–47, https://doi.org/10.1115/1.2929216.
[7] H. Weigl, J. Paduano, L. Frechette, A. Epstein, E. Greitzer, M. Bright, A. Strazisar, Active stabilization of rotating stall and surge in a transonic single-stage axial compressor, J. Turbomach. 120 (4) (1998) 625–636, https://doi.org/10.1115/1.2841772.
[8] I. Day, T. Breur, J. Escuret, M. Cherrett, A. Wilson, Stall inception and the prospects for active control in four high speed compressors, J. Turbomach. 121 (1) (1999) 18–27, https://doi.org/10.1115/1.2841229.
[9] J. Day, Stall, surge, and 75 years of research, J. Turbomach. 138 (1) (2016) 011001, https://doi.org/10.1115/1.4031473.
[10] X. Sun, X. Dong, D. Sun, Recent development of casing treatments for aeroengine compressors, Chin. J. Aeronaut. 32 (1) (2019) 1–36, https://doi.org/10.1016/j.cja.2018.11.005.
[11] C.C. Koch, Experimental Evaluation of Outer Case Blowing or Bleeding of Single Stage Axial Flow Compressor, part VI final report, Report No.: NASA CR-54592, NASA, Washington, D.C., 1970.

[12] H. Fujita, H. Takata, A study on configurations of casing treatment for axial flow compressors, Bull. JSME 27 (230) (1984) 1675–1681, https://doi.org/10.1299/jsme1958.27.1675.
[13] E.M. Greitzer, Review-axial compressor stall phenomena, J. Fluids Eng. 102 (2) (1980) 134–151, https://doi.org/10.1115/1.3240634.
[14] H. Takata, H. Tsukuda, Stall margin improvement by casing treatment - its mechanism and effectiveness, J. Eng. Power 99 (1) (1977) 121–133, https://doi.org/10.1115/1.3446241.
[15] G.D.J. Smith, N.A. Cumpsty, Flow phenomena in compressor casing treatment, J. Eng. Gas Turbines Power 106 (3) (1984) 532–541, https://doi.org/10.1115/1.3239604.
[16] A. Azimian, R. Elder, A. Mckenzie, Application of Recess Vaned Casing Treatment to Axial Flow Fans, ASME-89-GT-68, 1989.
[17] M. Ziabasharhagh, A.B. McKenzie, R.L. Elder, Recess Vane Passive stall control, ASME 92-GT-36, 1992.
[18] C. Kang, A. McKenzie, R. Elder, Recessed casing treatment effects on fan performance and flow field, in: International Gas Turbine and Aeroengine Congress and Exposition, Houston, Texas, June 5-8, 1995.
[19] G. Pullan, A. Young, I. Day, E. Greitzer, Z. Spakovszky, Origins and structure of spike-type rotating stall, J. Turbomach. 137 (5) (2015) 051007, https://doi.org/10.1115/1.4028494.
[20] T. Camp, I. Day, A study of spike and modal stall phenomena in a low speed axial compressor, J. Turbomach. 120 (3) (1998) 393–401, https://doi.org/10.1115/1.2841730.
[21] H. Vo, C. Tan, E. Greitzer, Criteria for spike initiated rotating stall, J. Turbomach. 130 (1) (2008) 011023, https://doi.org/10.1115/1.2750674.
[22] X.C. Mao, B. Liu, T.Q. Tang, H. Zhao, The impact of casing groove location on the flow instability in a counter-rotating axial flow compressor, Aerosp. Sci. Technol. 76 (2020) 250–259, https://doi.org/10.1016/j.ast.2018.01.037.
[23] Y. Sakuma, T. Watanabe, T. Himeno, D. Kato, T. Murooka, Y. Shuto, Numerical analysis of flow in a transonic compressor with a single circumferential casing groove: influence of groove location and depth on flow instability, J. Turbomach. 136 (3) (2013) 031017, https://doi.org/10.1115/1.4025575.
[24] J. Du, J. Li, L. Gao, F. Lin, J. Chen, The impact of casing groove location on stall margin and tip clearance flow in a low-speed axial compressor, J. Turbomach. 138 (12) (2016) 121007, https://doi.org/10.1115/1.4033472.
[25] M. Rolfes, M. Lange, K. Vogeler, R. Mailach, Experimental and numerical investigation of a circumferential groove casing treatment in a low-speed axial research compressor at different tip clearances, J. Turbomach. 139 (12) (2017) 121009, https://doi.org/10.1115/1.4037822.
[26] A. Shabbir, J.J. Adamczyk, Flow mechanism for stall margin improvement due to circumferential casing grooves on axial compressors, J. Turbomach. 127 (4) (2004) 708–717, https://doi.org/10.1115/1.2008970.
[27] T. Houghton, I. Day, Enhancing the stability of subsonic compressors using casing grooves, J. Turbomach. 133 (2) (2010) 021007, https://doi.org/10.1115/1.4000569.
[28] X. Sun, D. Sun, X. Liu, W. Yu, X. Wang, Theory of compressor stability enhancement using novel casing treatment, part 1: methodology, J. Propuls. Power 30 (5) (2014) 1224–1235, https://doi.org/10.2514/1.B34900.
[29] D. Sun, X. Liu, D. Jin, X. Gui, X. Sun, A theory of compressor stability enhancement using novel casing treatment, part 2: experiment, J. Propuls. Power 30 (5) (2014) 1236–1247, https://doi.org/10.2514/1.B34901.
[30] D. Sun, C. Nie, X. Liu, F. Lin, X. Sun, Further investigation on transonic compressor stall margin enhancement with stall precursor-suppressed casing treatment, J. Turbomach. 138 (2) (2015) 021001, https://doi.org/10.1115/1.4031775.
[31] X. Dong, D. Sun, F. Li, X. Sun, Stall margin enhancement of a novel casing treatment subjected to circumferential pressure distortion, Aerosp. Sci. Technol. 73 (2018) 239–255, https://doi.org/10.1016/j.ast.2017.12.005.
[32] J. Paduano, E. Greitzer, A. Epstein, Compression system stability and active control, Annu. Rev. Fluid Mech. 33 (2001) 491–517, https://doi.org/10.1146/annurev.fluid.33.1.491.
[33] C. Tan, I. Day, S. Morris, A. Wadia, Spike-type compressor stall inception, detection, and control, Annu. Rev. Fluid Mech. 42 (2010) 275–300, https://doi.org/10.1146/annurev-fluid-121108-145603.
[34] T. Pan, Q. Li, W. Yuan, H. Lu, Effects of axisymmetric arc-shaped slot casing treatment on partial surge initiated instability in a transonic axial flow compressor, Aerosp. Sci. Technol. 69 (2017) 257–268, https://doi.org/10.1016/j.ast.2017.05.036.
[35] J. Yu, E. Nesbitt, H. Kwan, S. Uellenberg, E. Chien, J. Premo, M. Ruiz, M. Czech, Quiet technology demonstrator 2 intake liner design and validation, in: 27th AIAA Aeroacoustics Conference, Cambridge, Massachusetts, May 08-10, AIAA 2006-2458, 2006.
[36] D.L. Sutliff, M.G. Jones, Low-speed fan noise attenuation from a foam-metal liner, J. Aircr. 46 (4) (2009) 1381–1394, https://doi.org/10.2514/1.41369.
[37] D.L. Sutliff, M.G. Jones, T.C. Hartley, High-speed turbofan noise reduction using foam-metal liner over-the-rotor, J. Aircr. 50 (5) (2013) 1491–1503, https://doi.org/10.2514/1.C032021.
[38] B. Walker, A. Hersh, L. Heidelberg, D. Sutliff, M. Spencer, Active resonators for control of multiple spinning modes in an axial flow fan inlet, in: Aerosp. 5th AIAA/CEAS Aeroacoustics Conference and Exhibit, Bellevue,WA, May 10-12, AIAA 99-1853, 1999.
[39] D. Zhao, C. Ji, L. Ang, Aeroacoustics comparison of double- and single-layer perforated liners in presence of joint bias-grazing flow, in: 2018 AIAA/CEAS Aeroacoustics Conference, Atlanta, Georgia, June 25-29, AIAA 2018-4099, 2018.
[40] R. Bozak, R. Dougherty, Measurement of noise reduction from acoustic casing treatments installed over a subscale high bypass ratio turbofan rotor, in: 2018 AIAA/CEAS Aeroacoustics Conference, Atlanta, Georgia, June 25-29, AIAA 2018-4099, 2018.
[41] R. Bozak, M. Jones, B. Howerton, M. Brown, Effect of grazing flow on grooved over-the-rotor acoustic casing treatments, in: 25th AIAA/CEAS Aeroacoustics Conference, Delft, The Netherlands, May 20-23, AIAA 2019-2580, 2019.
[42] S. Cabre, B. Tester, R. Astley, R. Bozak, Modelling of over-the-rotor acoustic treatments for improved noise suppression in turbofan engines, in: 25th AIAA/CEAS Aeroacoustics Conference, Delft, The Netherlands, May 20–23, AIAA 2019-2580, 2019.
[43] S. Singh, N. Bhatnagar, A survey of fabrication and application of metallic foams, J. Porous Mater. 25 (2018) 537–554, https://doi.org/10.1007/s10934-017-0467-1.
[44] M. Inoue, M. Kuroumaru, Structure of tip clearance flow in an isolated axial compressor rotor, J. Turbomach. 111 (7) (1989) 250–256, https://doi.org/10.1115/1.3262263.
[45] S. Weichert, I.J. Day, Detailed measurements of spike formation in an axial compressor, J. Turbomach. 136 (5) (2014) 051006, https://doi.org/10.1115/1.4025166.